Supporting Information

Enhancing Near-Infrared II Photothermal Conversion through Anchoring Numerous Nanospheres to the Edge of a Gold Nanosheet

Yajie Kong,[a†] Qi He,[b†] Heng Zhang,[c†] Haoyu Sun,[a] Yi Wang,[b*] Xiaohu Wu,[d*] Yanyun Ma,[e] and Yiqun Zheng[a*]

[a] School of Chemistry, Chemical Engineering, and Materials, Jining University, Qufu, Shandong 273155, China

[b] Chongqing Key Laboratory of Green Synthesis and Applications, College of Chemistry, Chongqing Normal University, Chongqing 401331, P. R. China

[c] School of Energy, Changzhou University, Changzhou, Jiangsu 213164, China

[d] Thermal Science Research Center, Shandong Institute of Advanced Technology, Jinan, Shandong 250100, China

[e] Institute of Functional Nano&Soft Materials (FUNSOM), Jiangsu Key Laboratory of Advanced Negative Carbon Technologies, Soochow University, Suzhou, Jiangsu 215123, China

[†] These authors contribute equally to this work.

[*] Corresponding author: Prof. Dr. Y. Zheng, E-mail: yzheng@jnxy.edu.cn; Prof. Y. Wang, ywang@cqnu.edu.cn; Prof. X. Wu, xiaohu.wu@iat.cn
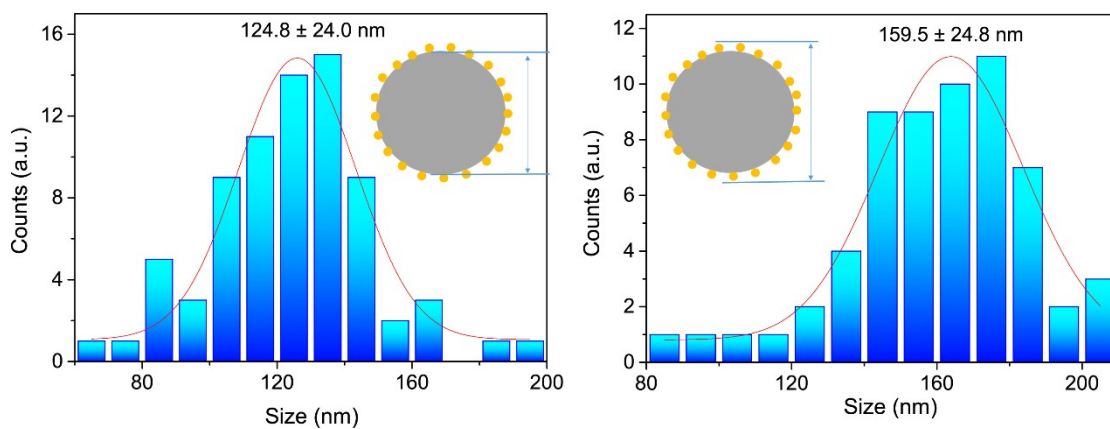
Figure S1. Histogram showing the size distribution of products shown in Figure 1g ($Au_{92.7}Se_{7.3}$ HNSs).
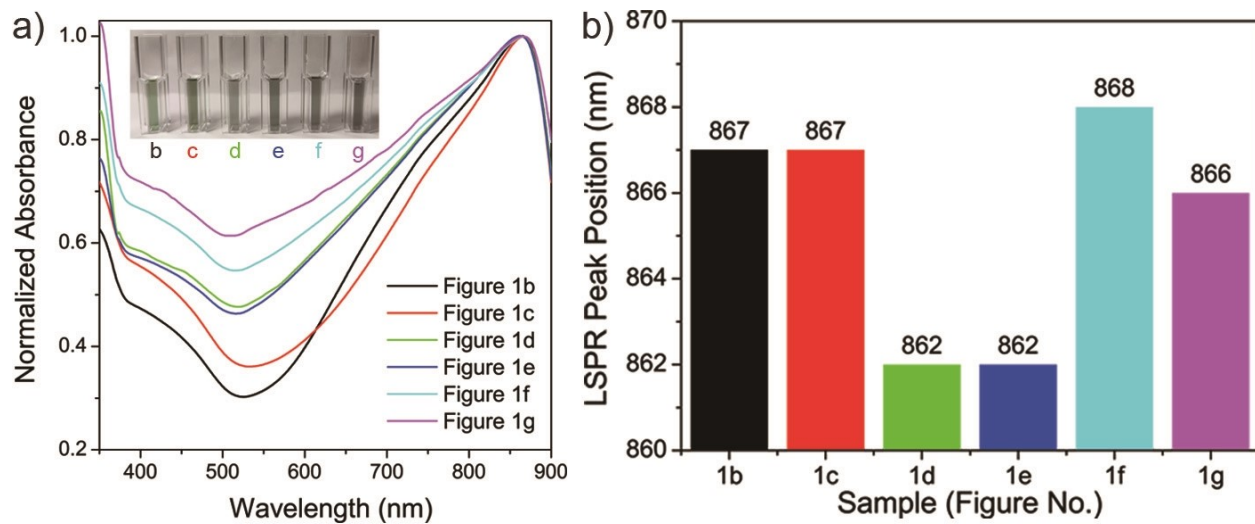
Figure S2. a) UV-vis extinction spectra and b) LSPR peak positions of products shown in Figure 1.
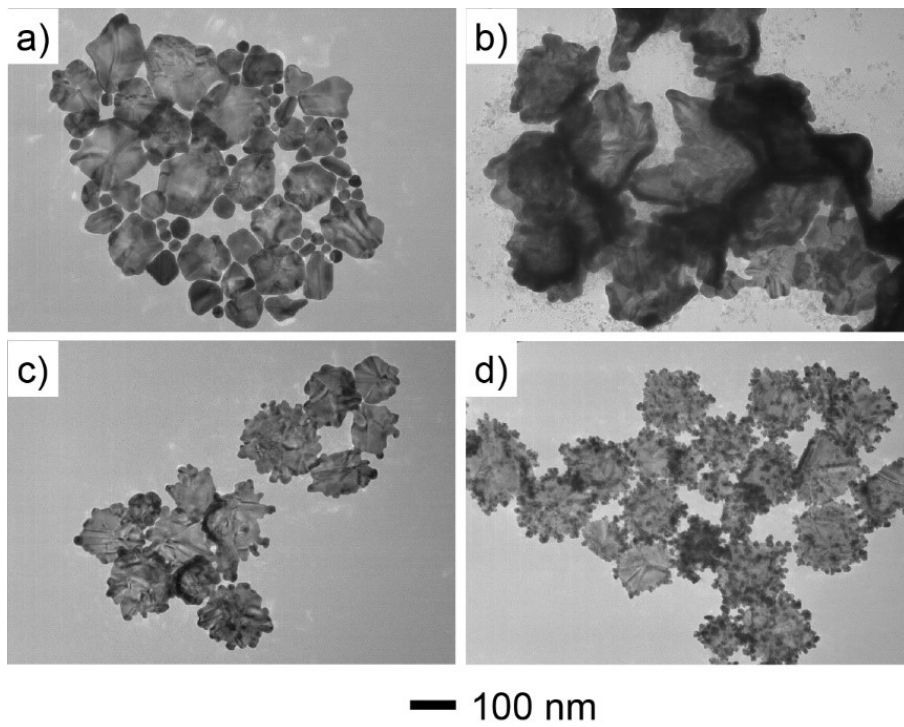
Figure S3. TEM images of products obtained via the standard procedure, except that the amount of SeO$_2$ was controlled to be a) 0, b) 0.1 μmol, c) 0.2 μmol, and d) 2 μmol, respectively.

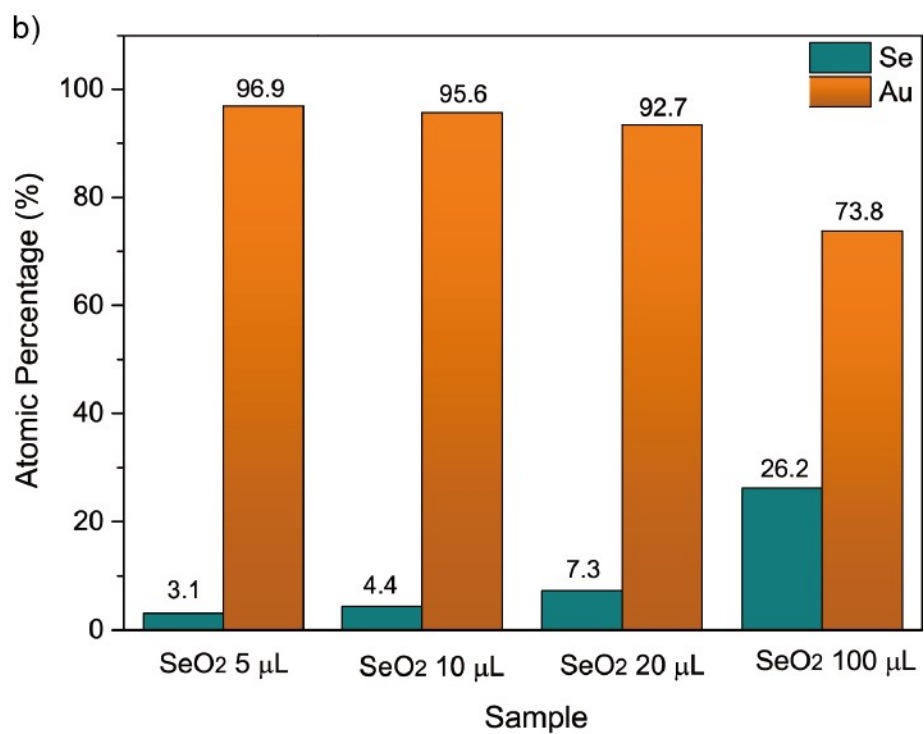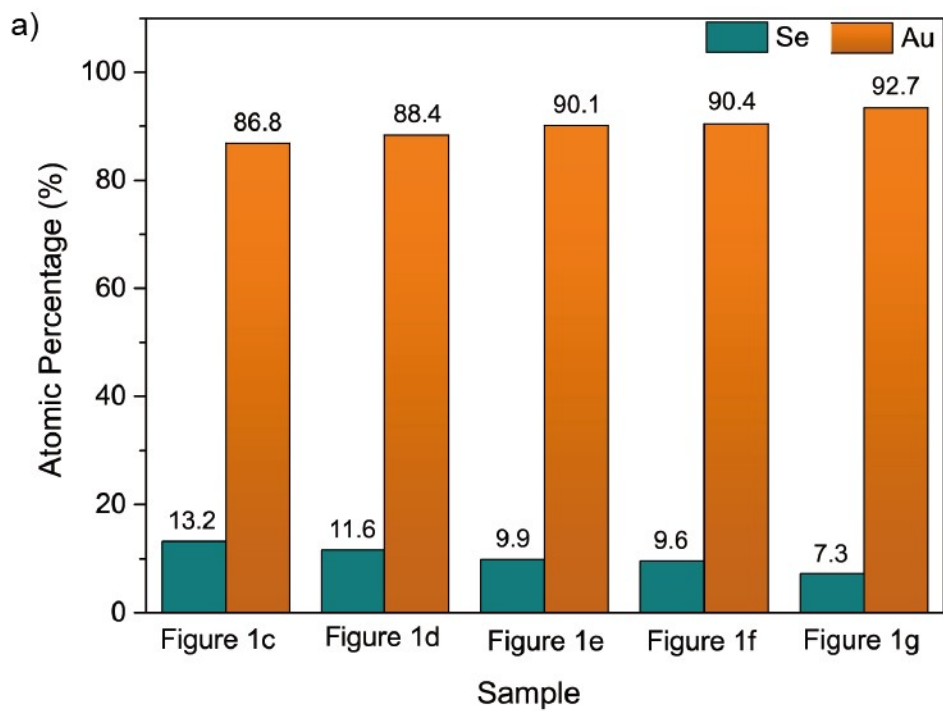**Figure S4. (**a) Histogram showing the elemental composition in Figure 1. (b) Histogram showing the elemental composition of AuSe HNSs with different volumes of SeO_2 (20 mM).
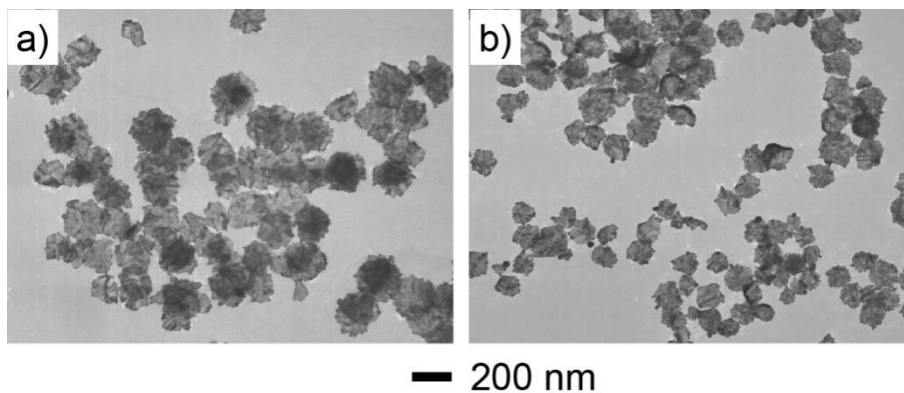
Figure S5. TEM images of AuSe products obtained *via* the standard procedure, except that the CTAC (200 mM, 1.5 mL) was replaced by: (a) CTAC (200 mM, 1.5 mL) + CTAB (200 mM, 0.5 mL), (b) CTAB (200 mM, 0.5 mL) + H$_2$O 1.5 mL.
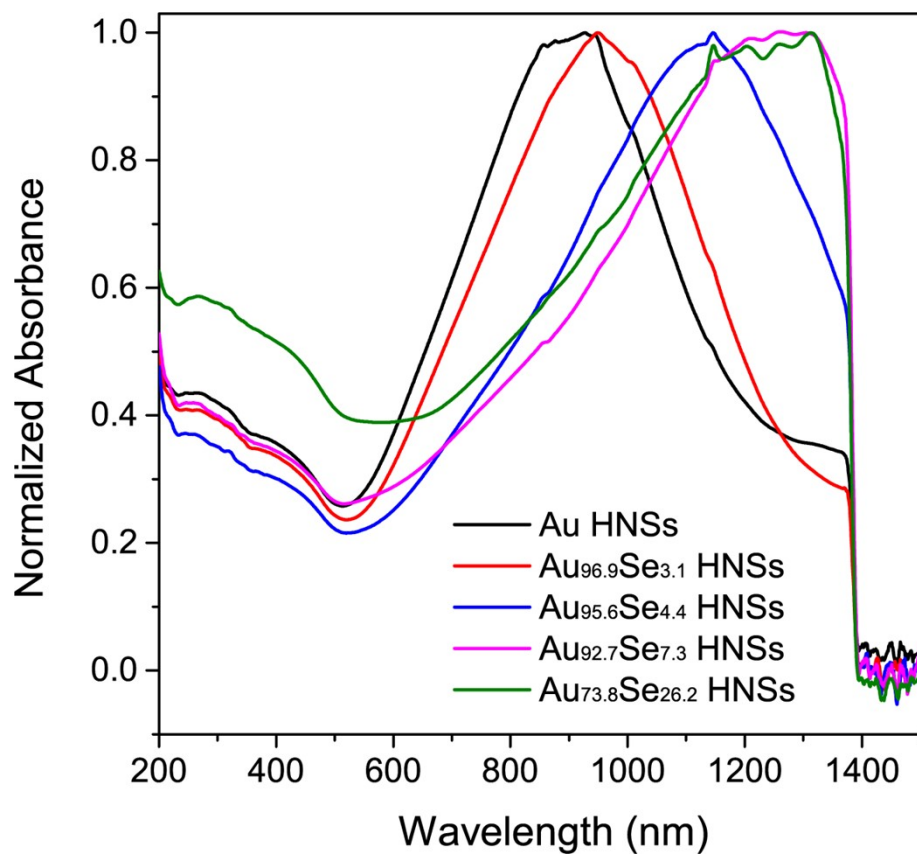
Figure S6. UV-vis-NIR absorption of products shown in Figure 4a.
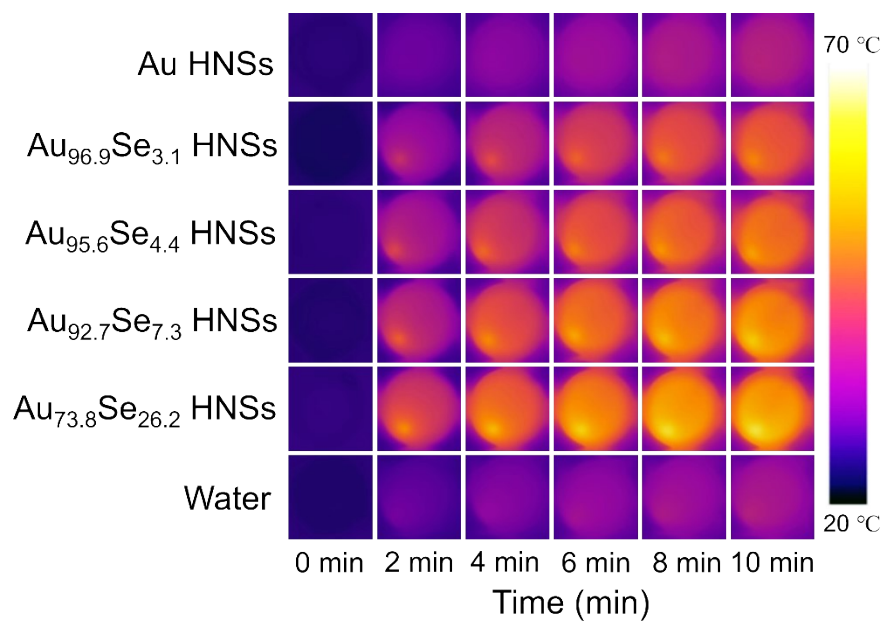
Figure S7. Photothermal images of five Au-based nanosheets upon irradiation.
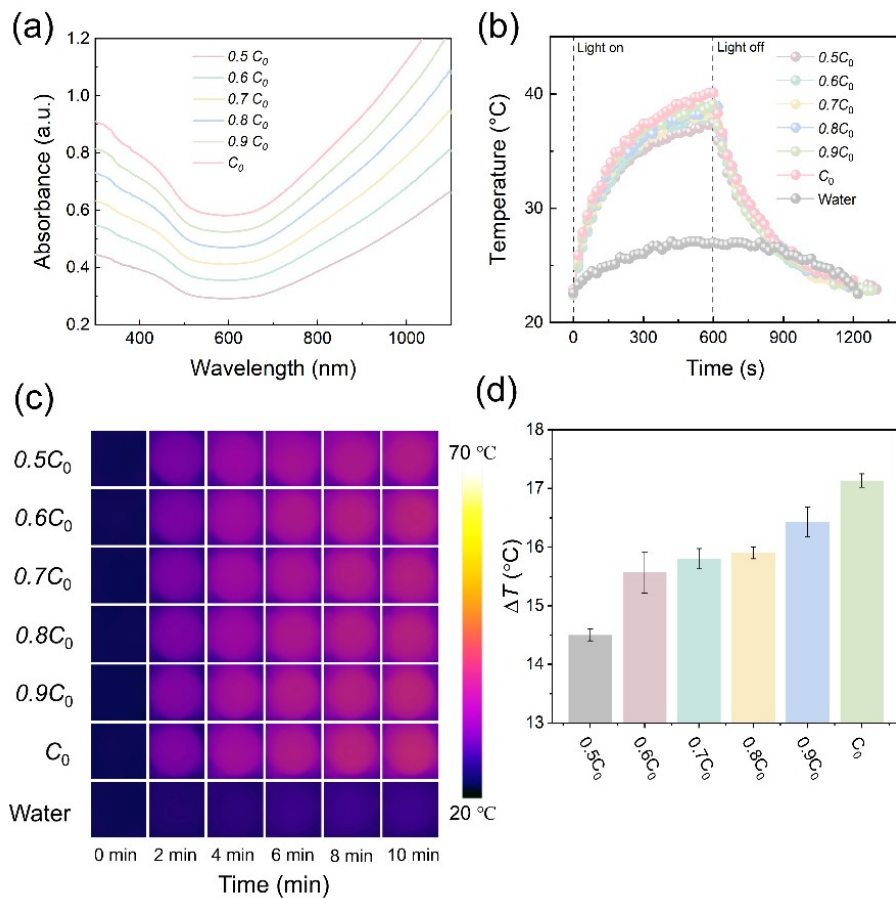
Figure S8. Photothermal conversion performances of $Au_{73.8}Se_{26.2}$ HNSs at different particle concentrations: (a) UV-Vis-NIR absorption spectra; (b) $\varDelta T$-t curves collected with a 1064 nm laser on/off (1 W cm^{-2}); (c) corresponding thermal images; (d) Histogram of $\varDelta T$.
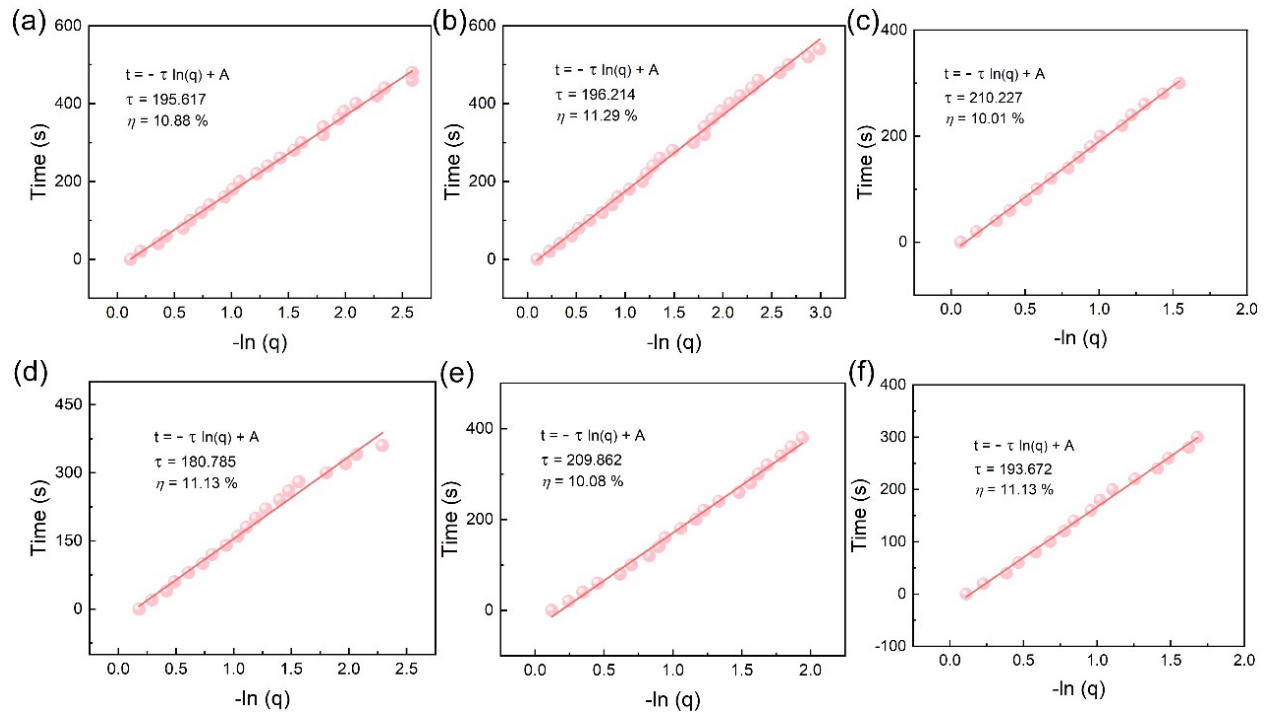
Figure S9. Linear fitting plot of ln(q)-time during the cooling period. C = (a) $0.5C_0$ (b) $0.6C_0$ (c) $0.7C_0$ (d) $0.8C_0$ (e) $0.9C_0$ and (f) C_0.

Figure S10. Optical parameters of the materials. (a) Refractive index and (b) Extinction coefficient.

Figure S11. Temperature distributions of nanoparticles with different Au-Se ratios. (a) *x*-axis,

(b) *y*-axis, c) *z*-axis.

Table S1. Real-time temperatures of the water and product solutions as monitored by the thermal imaging camera.

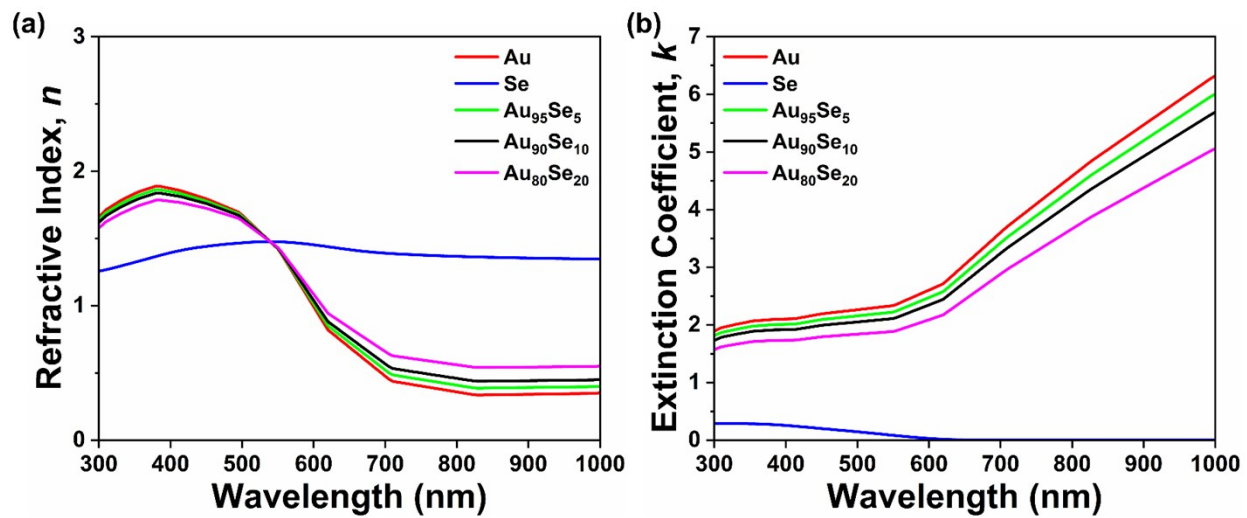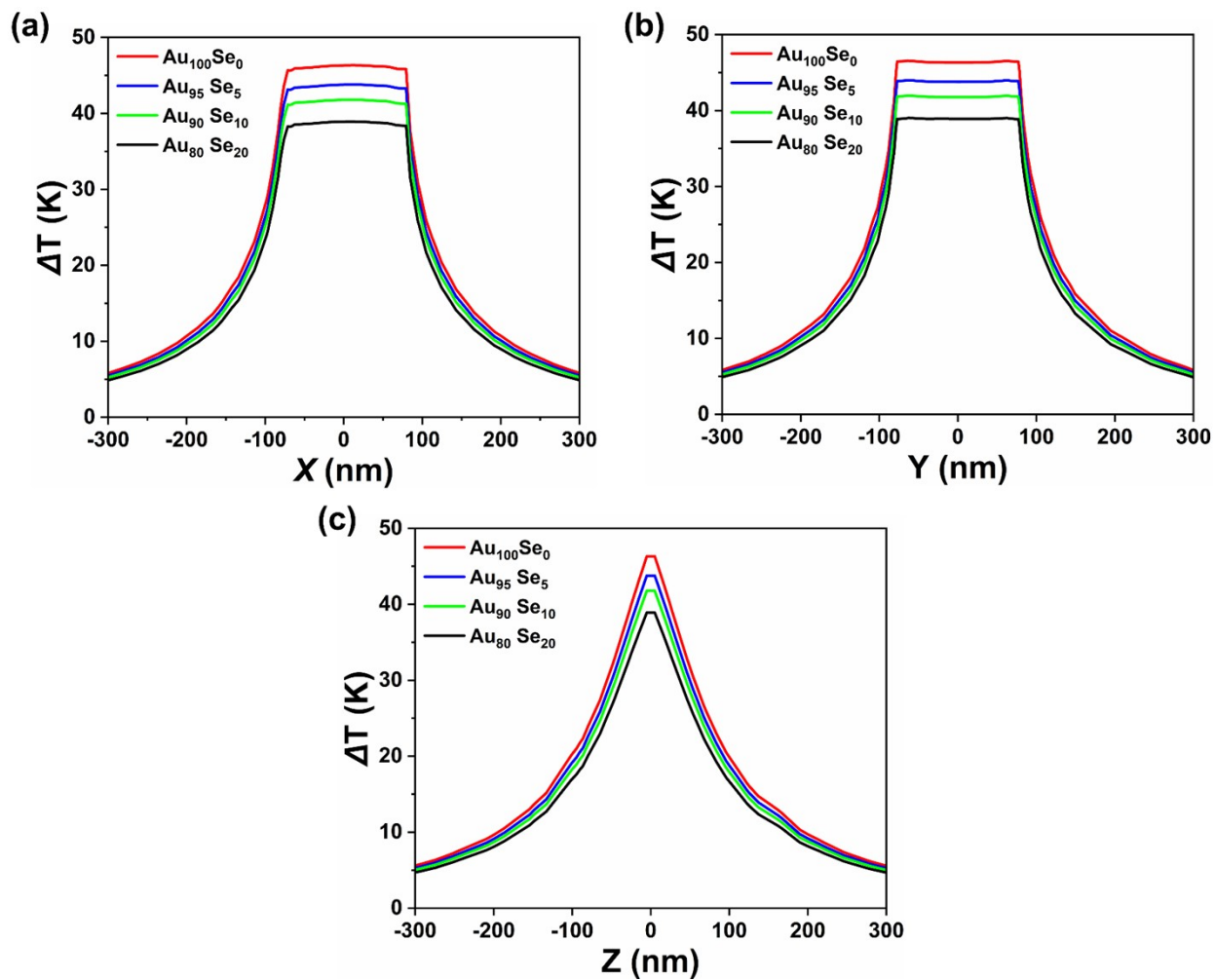| Time (s)	T_{H2O} (°C)	ΔT_{H2O}	$T_{product}$ (°C)	$\Delta T_{product}$	$\Delta T/\Delta T_{max}$	$-\ln(\Delta T/\Delta T_{max})$
0	24.7	0	25.7	0	0	/
20	26.2	1.5	32.3	6.6	0.2260274	1.48709906
40	27.3	2.6	34.9	9.2	0.3150685	1.154965225
60	28.3	3.6	37.3	11.6	0.3972603	0.923163611
80	28.7	4	39.5	13.8	0.4726027	0.749500117
100	29.2	4.5	41.1	15.4	0.5273973	0.6398012
120	29.7	5	42.3	16.6	0.5684932	0.564766014
140	29.9	5.2	43.8	18.1	0.619863	0.478256771
160	30.4	5.7	44.4	18.7	0.640411	0.445645185
180	31.1	6.4	45.6	19.9	0.6815068	0.383448978
200	31.8	7.1	46	20.3	0.6952055	0.363547823
220	32	7.3	46.9	21.2	0.7260274	0.320167528
240	32.5	7.8	47.3	21.6	0.739726	0.301475395
260	32.7	8	48.4	22.7	0.7773973	0.251803785
280	33.2	8.5	48.8	23.1	0.7910959	0.234336092
300	33.3	8.6	49.4	23.7	0.8116438	0.208693661
320	33.6	8.9	49.7	24	0.8219178	0.196114879
340	34.2	9.5	50.2	24.5	0.8390411	0.175495592
360	34.6	9.9	50.6	24.9	0.8527397	0.159300906
380	34.8	10.1	51.4	25.7	0.880137	0.127677717
400	34.9	10.2	51.3	25.6	0.8767123	0.131576358
420	35.2	10.5	51.9	26.2	0.8972603	0.108409299
440	35.4	10.7	52.3	26.6	0.9109589	0.093257493
460	35.5	10.8	52	26.3	0.9006849	0.10459977
480	35.7	11	52.5	26.8	0.9178082	0.085766822
500	36	11.3	53.5	27.8	0.9520548	0.049132689
520	36.2	11.5	54	28.3	0.9691781	0.031306905

540	36.4	11.7	54.3	28.6	0.9794521	0.020761991
560	36.6	11.9	54.7	29	0.9931507	0.006872879
580	36.8	12.1	54.7	29	0.9931507	0.006872879
600	**37.1**	**12.4**	**54.9**	**29.2**	**1**	**0**
620			50.5	24.8	0.8493151	0.163325056
640			48.4	22.7	0.7773973	0.251803785
660			47	21.3	0.7294521	0.315461637
680			45.6	19.9	0.6815068	0.383448978
700			44.7	19	0.6506849	0.42972973
720			43.6	17.9	0.6130137	0.489367996
740			42.9	17.2	0.5890411	0.529259325
760			41.7	16	0.5479452	0.601579987
780			40.8	15.1	0.5171233	0.659473965
800			40.3	14.6	0.5	0.693147181
820			39.6	13.9	0.4760274	0.742279869
840			39	13.3	0.4554795	0.786404674
860			38.2	12.5	0.4280822	0.848440065
880			37.5	11.8	0.4041096	0.906069178
900			36.9	11.2	0.3835616	0.958254931
920			36.2	10.5	0.359589	1.022793452
940			35.5	9.8	0.3356164	1.091786324
960			35.1	9.4	0.3219178	1.13345902
980			34.6	8.9	0.3047945	1.188117433
1000			34.2	8.5	0.2910959	1.234102546
1020			33.7	8	0.2739726	1.294727168
1040			33.4	7.7	0.2636986	1.33294838
1060			32.8	7.1	0.2431507	1.414073925
1080			32.5	6.8	0.2328767	1.457246097
1100			32.6	6.9	0.2363014	1.442647298
1120			31.7	6	0.2054795	1.58240924
1140			31.5	5.8	0.1986301	1.616310792

1160	30.8	5.1	0.1746575	1.74492817
1180	30.5	4.8	0.1643836	1.805552791
1200	30.3	4.6	0.1575342	1.848112406
1220	30.3	4.6	0.1575342	1.848112406
1240	29.8	4.1	0.140411	1.963181736
1260	29.6	3.9	0.1335616	2.013192156
1280	29.5	3.8	0.130137	2.039167643
1300	29.3	3.6	0.1232877	2.093234864
1320	29	3.3	0.1130137	2.180246241
1340	28.4	2.7	0.0924658	2.380916936
1360	28.2	2.5	0.0856164	2.457877977
1380	28	2.3	0.0787671	2.541259586
1400	28.2	2.5	0.0856164	2.457877977
1420	28	2.3	0.0787671	2.541259586
1440	27.8	2.1	0.0719178	2.632231365
1460	27.6	1.9	0.0650685	2.732314823
1480	27.4	1.7	0.0582192	2.843540458
1500	27.4	1.7	0.0582192	2.843540458
1520	27.1	1.4	0.0479452	3.037696473
1540	27	1.3	0.0445205	3.111804445
1560	26.9	1.2	0.0410959	3.191847152
1580	26.7	1	0.0342466	3.374168709
1600	26.7	1	0.0342466	3.374168709
1620	26.5	0.8	0.0273973	3.597312261
1640	26.3	0.6	0.0205479	3.884994333
1660	26.3	0.6	0.0205479	3.884994333
1680	26.2	0.5	0.0171233	4.06731589
1700	26	0.3	0.010274	4.578141514
1720	25.9	0.2	0.0068493	4.983606622

Table S2. Calculation of the resulting photothermal conversion efficiency on the basis of the initial processing of the data.

τ	$A1064_{nm}$	ΔT_{maxH_2O}	$\Delta T_{max\ product}$	hA（$=m*Cp/\tau$）	η
354.758	0.7113	12.4	29.2	0.020126396	41.97%

Table S3. Summary of XRD results of Au NSs, Se-doped Au NSs, and AuSe HNSs.

Sample No.	Crystal Plane	Two Theta (^{o})	Full width at half maxima (FWHM, ^{o})	Crystalline Size[*] (nm)
Au NSs	(111)	37.859	0.440	18.93
Se-doped Au NSs	(111)	37.794	0.653	12.75
$Au_{92.7}Se_{7.3}$ HNSs	(111)	37.861	0.425	19.60

[*]Crystalline size was calculated using Debye-Scherrer equation.

Table S4. Summary of the relative peak areas (%) for each split B.E. peak and the parameters used to fit the Se 3d and Au 4f high-resolution XPS spectra.

Orbital	B. E. Peak (eV)	FWHM (eV)	relative peak area	element/oxidation state
Se 3d	54.5	1.99	32.8%	Se(0)
	55.7	1.73	8.1%	Se(II)
	57.4	4.56	53.9%	Se(0)
	61.4	3.57	5.2%	Se(II)
Au 4f	83.3	0.85	44.4%	Au(0)
	84.7	1.48	9.9%	Au(I)
	87.5	0.86	42.4%	Au(0)
	88.4	1.58	3.3%	Au(I)